ELSEVIER

Contents lists available at ScienceDirect

Composites Science and Technology

journal homepage: www.elsevier.com/locate/compscitech





Engineering the electrospinning of MWCNTs/epoxy nanofiber scaffolds to enhance physical and mechanical properties of CFRPs

Vidya Wable ^{a,1}, Pias Kumar Biswas ^{a,1}, Reza Moheimani ^a, Nojan Aliahmad ^a, Peter Omole ^a, Amanda P. Siegel ^{a,b}, Mangilal Agarwal ^{a,**}, Hamid Dalir ^{a,*}

ARTICLE INFO

Keywords:
MWCNTs/epoxy nanofibers
Electrospinning
Nanofiber scaffolds
Thermal/mechanical/electrical properties
Enhanced composites

ABSTRACT

A cost-effective approach to improve the physical and mechanical properties of carbon fiber reinforced polymer (CFRP) prepreg composites, where electrospun multiwalled carbon nanotubes (MWCNTs)/epoxy nanofibers were synthesized and incorporated in between the layers of conventional CFRP prepreg composite has been presented. MWCNT-aligned epoxy nanofibers were successfully produced by an optimized electrospinning process. Nanofibers were deposited directly onto prepreg layers to achieve improved adhesion and interfacial bonding, leading to added strength and improvements in other mechanical properties. Thus, interlaminar shear strength (ILSS) and fatigue performance at high-stress regimes increased by 29% and 27%, respectively. Barely visible impact damage (BVID) energy increased significantly by up to 45%. The thermal and electrical conductivities were also enhanced significantly due to the presence of the highly conductive MWCNT networks between the CFRP layers. The presented method was capable of uniformly depositing high contents of MWCNTs at interlaminar ply interface of prepregs to strengthen/enhance CFRP properties, which has not been previously shown to be possible due to high resin viscosity caused by randomly oriented MWCNTs in epoxy system.

1. Introduction

Carbon fiber reinforced polymer (CFRP) composites are used extensively in the aeronautical, automotive, wind turbine, marine appliances, and conventional building construction due to their specific stiffness to strength ratio, light weight, corrosion resistance, fatigue performance, superior electro-mechanical properties, and most important, ease of application [1–7]. Despite having high weatherability, environment friendliness, and qualities unlike traditional metal and alloys, CFRP suffers from major drawbacks in the form of matrix fracturing, multiple delamination, and fiber breakage, which are a particular liability, for example, in aerospace industries [1,8–10]. CFRP/epoxy laminate is a composite material composed of the resin matrix and carbon fiber reinforcement stacked layer by layer where the thermosetting polymer matrix has significant influence over the strength and flexural rigidity of the composite [11]. When compressive stress is applied, the combination of shear delamination and fiber damage can

cause a major adverse impact on the overall performance. In fact, the enhancement of flexural strength by altering polymer structure has been a major challenge over the last decade. Several studies have demonstrated that the addition of nano-carbonaceous material (SWCNT [12], MWCNT [13], Graphene [14], etc.) to nanocomposites leads to improved physical properties, making it possible for novel features not available in the original materials to be developed to satisfy the requirements of a variety of CFRP applications. However, computational studies have also demonstrated that the mechanical competence of nanocomposites can be significantly improved and tuned for specific applications given bioinspired design motifs are wisely employed [15, 16].

Electrospinning, an easy and simple technique for producing nanofibers [17–20], is progressing fast along two major directions. One is the manufacturing on a broad scale for promising commercial industries [21–23]. The other is traditional single-fluid blending electrospinning [24] which is categorized further into different types of double-fluid and

^a Integrated Nanosystems Development Institute, Purdue School of Engineering and Technology, Indiana University—Purdue University Indianapolis, Indianapolis, IN, 46202. USA

^b Multiscale Integrated Technology Solutions LLC, Indianapolis, IN, 46202, USA

^{*} Corresponding author.

^{**} Corresponding author.

E-mail addresses: agarwal@iupui.edu (M. Agarwal), hdalir@iupui.edu (H. Dalir).

¹ These authors contributed equally.

three-fluid methods. Depending on the spatial points, there are two kinds of double-fluid electrospinning, i.e., coaxial electrospinning [25] and side-by-side electrospinning [26]. With regard to the three-fluid processes, there are tri-axial process in which tri-layer working fluids are placed in a coaxial manner [27], coaxial process with a side-by-side core, side-by-side process with one coaxial side, and tri-layer parallel side-by-side one. Complex multiple-fluid [28], solid needle [29] and free-surface processes [30], the polymers that can be electrospun into nanofibers are always the slightly over 100 types [31]. These advanced methods should significantly develop the competency of electrospinning in producing a wide range of complicated nanostructures. However, among all the complicated nanostructures, the fabrication of thermosetting nanofibers at nanoscale has never been accomplished. To do so, the recent phase of our study has been focused on carrying out the above-mentioned task [32]. we were capable of making thermosetting polymers spinnable by developing a partial curing strategy through a thermal treatment process, and characterization of submicron thermosetting filaments with embedded aligned MWCNTs networks.

Furthermore, nanofibers (NFs) with controllable alignment can be produced by modifying the electrospinning [33]. Electrospinning also can be used for the mass production of NFs because of the easy handling, possibility of control of the diameter, low cost, simple operation, and high reproducibility [34]. In brief, the characteristics of electrospun fibers can be controlled by electrospinning parameters, including the solution variables (e.g., surface tension, viscosity, and conductivity), operating variables (e.g., applied voltage, spinning distance, and solution flow rate), reviewed these factors for sensor and battery studies [35, 36].

Numerous studies to produce electrospun epoxy-CNT composite materials have been reported, where the thermosetting polymer is typically mixed with a thermoplastic polymer to make the resulting mixture spinnable [37-40]. However, when those nanofibers are integrated into the laminated composites, the presence of thermoplastic materials brings significant adverse thermal and electrical effects and increases the potential for delamination between the layers. In the current study, the method of producing epoxy-MWCNT composites with different carbon nanotubes concentration (1-8 wt%) is demonstrated. Characterization by scanning electron microscopy (SEM) depict the nano scaffold structure of MWCNTs/epoxy electrospun nanofibers (ENFs) along with the cross-sectional view of laminated composites. Studies comparing the interlaminar shear strength, flexural and tensile properties and the fatigue of the resulting materials were undertaken before and after incorporation of MWCNTs/epoxy ENFs. Low-speed energy impact experiments were carried out to inflict barely visible impact damage (BVID) and to assess the impact reaction of CFRP laminates. As shown before, MWCNTs significantly improve thermal conductivity, electrical conductivity and electromagnetic interference shielding (EMI) of CFRP laminated structures [41-43], here these properties were also assessed before and after incorporation of the MWCNTs/epoxy ENFs.

2. Experimental

2.1. Solution preparation

A masterbatch of non-functionalized MWCNTs was used as nanoreinforcements to be mixed with epoxy. The masterbatch consists of epoxy resin based on Bisphenol A (50–99 pbw. %), ethanol solvent (<15% volume) and carbon nanotubes (5 wt%) (NanocylTM S.A., Belgium). The mixture was diluted with neat epoxy (Miller-Stephenson, USA) in the presence of dimethylformamide (DMF) and Triton X- 100 to obtain 2, 4, and 8 wt% MWCNT content. To achieve a well-dispersed CNT polymer matrix, probe sonication was applied in steady time intervals. A curing agent was then added to the solution allowing it to rest for 20 h to create a semi-cured solution with the viscosity required for the electrospinning process. The solution was then degassed in a vacuum

oven to remove any trapped air bubbles. Syringes were filled with the final nanocomposite solution, and electrospinning was performed. The electrospinning process was optimized at 16 kV with the feeding rate, and needle gauge of 0.5 ml/h and 26 G, respectively. A stainless-steel collector was placed at 10 cm from the needle. The solution from the needle tip was deposited on a prepreg layer mounted on the metallic collector resulting in a formation of a MWCNTs/epoxy nanofiber scaffold.

2.2. Fabrication of composites and enhanced nanocomposite

The control and enhanced CFRP specimens for testing were fabricated from a hot melt epoxy-carbon fiber with a plain weave pattern (SE70 Gurit Holding AG, Wattwil/Switzerland). Here, symmetric, and balanced laminate ($100 \times 100 \text{ mm}^2$) stacks were made using a hand layup method followed by vacuum bagging to minimize void percentage within the [$0/90/\pm45$]_{2s} stacking sequence [44,45] in cure. For enhanced composites, MWCNTs/epoxy ENFs were deposited on the CF layers using the previously described optimized electrospinning method.

The size of the nanofibers and thickness of the electrospun scaffolds were adjusted without any interlayer deformation such that there was no issue in epoxy diffusion during composite fabrication. The final panel contained 8 layers of woven fabric for the control and 7 layers of epoxy-MWCNTs nanofibers for the enhanced composites. The control and enhanced composites were fully cured by placing them in a programmable oven (Easy Composite, UK) at 120 °C for 25 min while vacuuming under 1 bar. The samples were cooled down to room temperature while maintaining the pressure. Specimen thickness was measured to be 2 mm for all conditions. Fig. 1 shows step-by-step description of fabrication of short beam strength (SBS) composite specimens.

2.3. Mechanical properties and characterization

The specimens were cut by mill tool from the $100 \times 100 \text{ mm}^2$ fabricated composite panels [0/90/±45]_{2s}. Short Beam Shearing was carried out for inter-laminar bond strength characterization. Within the tight tolerances of the ASTM D2344, the final measurements of the samples were 2 mm \times 4 mm \times 12 mm (Fig. 2). The test was conducted on an Instron universal testing machine with a crosshead speed of 1.27 mm/min and a span-to-depth ratio of 4. For the short beam fatigue test, loads ranged from 60 to 90% of the ultimate strength, with an R-value of 0.1. To define the interlaminar shear strength, ten coupons cut from baseline (pristine) and electrospun 4 wt% MWCNTs composite panel were tested in static cyclic loading conditions. The average values from ten tests for each specimen and their standard deviations are reported in this study. Scanning electron microscopy (FESEM; JEOL 7800F, JEOL Japan) was used to interpret the fractured surfaces of the SBS samples and the morphology of MWCNTs/epoxy ENFs. Prior to SEM observation, a thin layer of gold coating was necessary to avoid the electrical charging of the specimen.

2.4. BVID

Barely visible impact damage (BVID) tests were carried out by a customized aluminum impactor bar with a spherical diameter of 10 mm, and having a weight, length and width of 325 g, 72.39 cm, and 1.27 cm, respectively. Variable nitrogen gas (N_2) pressures were used to apply force on the impactor. Specimens were fixed on a stand where a high-speed DSC-RX10 camera was used to record images, impactor displacement, and time per revolution. The tip of the impactor was marked red so that the very first displacement of the impactor could be easily detected. Recorded images were analyzed using Image-J software. The impact energy relationship per dent was applied to the control and enhanced CFRP and was calculated using the energy equation.

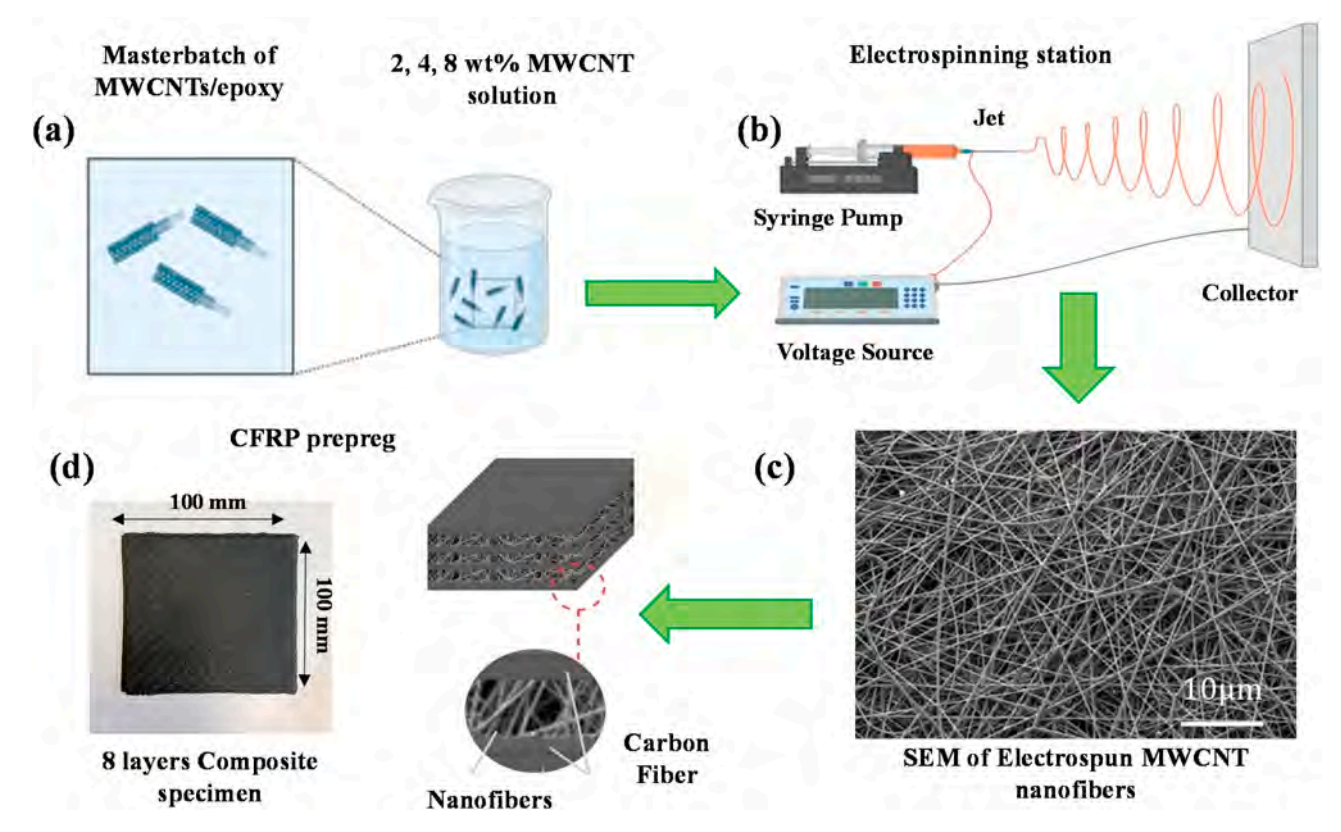


Fig. 1. Step-by-step description of fabrication of SBS composite specimens. a) A masterbatch of MWCNTs/epoxy is sonicated with epoxy and a curing agent to develop 2,4, or 8 wt% MWCNT solution. b) The MWCNT/epoxy mixture is electrospun onto CFRP prepreg. c) SEM of ENFs on CFRP prepreg d) CFRP prepreg with electrospun ENFs are heat/vacuum treated to generate a composite specimen eight layers thick for mechanical testing.

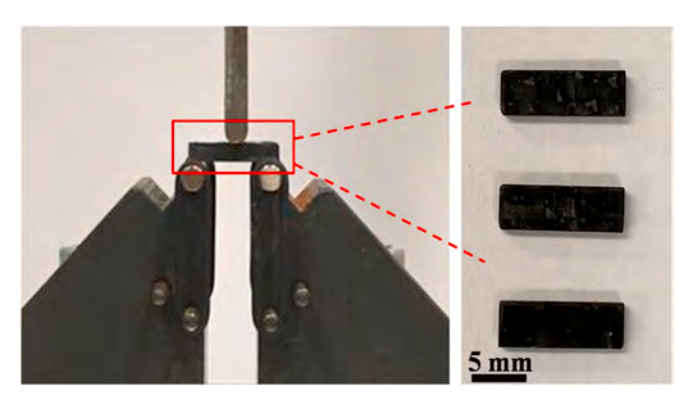


Fig. 2. Three-point bending test setup with coupon above the supporting pins.

2.5. Thermal Conductivity

The thermal conductivity was investigated at room temperature using a compact and versatile Hot Disk Thermal Constants Analyzer equipment (ThermTest TPS 500S, Sweden). To begin the experiment, two samples of the same dimensions are cut and made into a sandwiched structure around a thermistor (Kaptan 6 mm). This thermistor works as a heat sink and thermal sensor both at the same time. The specific power of 5 mW using direct current was applied across opposite ends of 5 laminated samples, and resultant temperature across the sample was measured after 5 ± 1 s.

2.6. Electrical Conductivity

The volume electrical resistivity of the laminated CFRP composites was measured by two probes using Impedance Spectroscopy (Hewlett

Packard 4192A LF impedance analyzer, USA) via their thickness according to ASTM D257-14 at temperature 22 °C and relative humidity 40%. The upper and lower surfaces of the composite samples were gently polished and coated with a silver paste to reduce surface resistivity. The copper tape was used as a conductor between the sample and the clamps of the system to maintain uniform contact with the surface. Sample resistance was measured in the frequency spectrum from 13 MHz to 5 Hz. As the difference between control and enhanced composite is very slight, the resistivity at 100 Hz was set as the resistance value.

2.7. EMI Shielding

Electromagnetic Interface shielding performance was evaluated based on the waveguide concept [46,47]. The equipment consisted of a hollow rectangular waveguide with an electrically conductive frame. The receiving antenna was located inside the waveguide while a sample was mounted at the entrance to the waveguide. A network analyzer (8719D Keysight, CA, USA) over the X-band frequency range (8.2 GHz–12.4 GHz) with a line scanning vibration of electrical field wave was used to produce the electromagnetic signals. The total EMI shielding effectiveness is a combination of three parts depending on its propagation properties. It can be written as EMI SE_T (dB) = 10 log (P_i/P_t) = EMI SE_A + EMI SE_R + EMI SE_M where SE_A, SE_R and SE_M correspond to the reflection, adsorption, and multi-reflections, respectively [48]. P_i the incident power, and P_t is the transmitted power of the electromagnetic waves. The following formulas were used to calculate their values:

EMI
$$SE_T = 10log \frac{1}{|S_{12}|^2} = 10log \frac{1}{|S_{21}|^2}$$
 (1)

EMI
$$SE_R = 10log \left(\frac{1}{1 - |S_{11}|^2}\right) = 10log \left(\frac{1}{1 - |S_{22}|^2}\right)$$
 (2)

EMI
$$SE_A = 10log \left(\frac{1 - |S_{11}|^2}{|S_{12}|^2}\right) = 10log \left(\frac{1 - |S_{22}|^2}{|S_{12}|^2}\right)$$
 (3)

Here S_{11} , S_{22} , S_{12} , and S_{21} are the complex scattering parameters that correspond to the surface reflection coefficients at both ends of the samples (S_{11} , S_{22}) and the transmission coefficients of the forward and reverse transmission of electromagnetic waves (S_{12} , S_{21}). Another segment SE_M is not considered when the EMI shielding effectiveness is more than 10 dB. All the above scattering parameters were calculated by the ratio of input voltage to the output voltage on the frequency distribution as the following equation:

$$S_{ab} = \frac{V_a^-}{V_+^+} \tag{4}$$

For example, S_{12} which is a transmission coefficient shows the input voltage of port 1 to the output voltage of port 2.

3. Results and discussion

3.1. Mechanical properties and morphology

The small dimensions of the Interlaminar Shear Strength (ILSS) test specimen along with the ease of testing make the test method more appealing than other shear tests [49]. Representative load-displacement curves and the corresponding ILSS values for each laminate configuration i.e., baseline, 2, 4, and 8 wt% MWCNTs are given in Fig. 3. The load increased with displacement in the linear elastic region until the peak load as shown in Fig. 3(a). Assuming the maximum shear stress creates cracking at the mid-plane position of the laminate, the ILSS of the laminate was determined using the maximum strength reached during

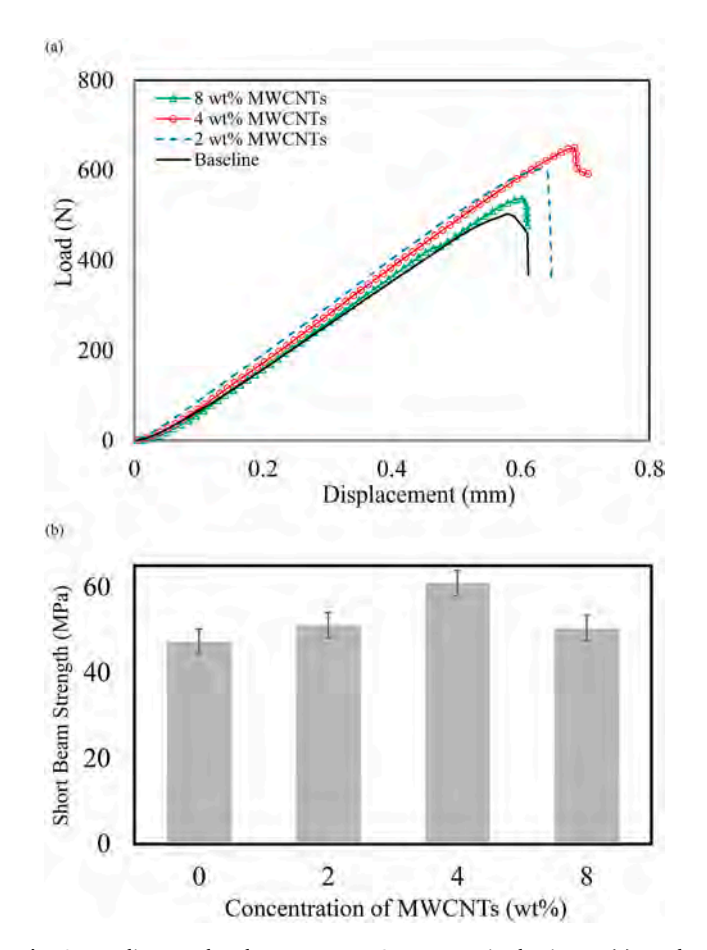


Fig. 3. Baseline vs. the electrospun MWCNT composite laminates (a) Load-displacement curves, (b) Short Beam Strength.

the tests. The reinforced matrix with 4 wt% of MWCNT ENFs indicates the highest load of 650.01 N and then dropped abruptly. The baseline sample (0 wt% MWCNT) has shown the lowest peak load, which was 503.92 N. However, it should be noted that the addition of 8 wt% of MWCNT ENFs decreased maximum shear strength compared to the other two ENFs samples. Previous studies showed a high concentration of MWCNTs may cause aggregation [50]. The MWCNT clusters prevent uniform dispersion of epoxy into fiber-matrix and result in poor performance [51]. SEM images will show later that the multiple cracks and pull-out fibers were observed near the mid-plane while the interface itself remained intact, showing that the ENFs reinforced region holds higher ILSS than the pristine interlayer. The ILSS or Short beam strength bar shown in Fig. 3(b) is average values of ten individually tested coupons for each laminate configuration. Reinforcing by the addition of 2, and 4 wt% MWCNT ENFs enhanced the ILSS by 8%, and 29%, respectively. As discussed, there was a slight decline with 8 wt% MWCNTs compared to 2 and 4 wt% due to nonuniform dispersion and void formation.

Based on the enhanced properties of the 4 wt% MWCNTs, it was chosen for further mechanical testing in comparison with the baseline samples. Fatigue experiments, which were the same as static specimens, were manufactured and their fatigue lives were evaluated. An Instron Co. 8801 fatigue tester was used for the fatigue test and the stress ratio (R) and frequency of the fatigue tests were set to be 0.1 and 5 Hz, respectively. Fig. 4 shows the S-N curves of short beam tests for control samples and 4 wt% MWCNT. All the specimens used in the fatigue tests failed at the center of their gauge length where the impact damage was found. In all cases, the MWCNT reinforced specimens showed longer fatigue lives. Also, the fatigue enhancement of coupons with 4 wt% MWCNTs were in the range of 25–60% with respect to the baseline.

These results suggested that the addition of 4 wt% MWCNTs has a significant effect on the strength of the composite structure under cyclic loading. Next, enhancements to interlaminar properties were examined. The flexural test is technically the most practical for evaluating matrices and fiber–resin interface in composites. Fig. 5 shows the flexural strength and modulus of the baseline and electrospun composite laminates. The flexural strength and strain of the enhanced 4 wt% MWCNT composited was higher in comparison with those of baseline. Others have reported that when nano reinforcements were incorporated, a significant increase in the flexural properties has been observed [52–54]

Here, incorporation of electrospun MWCNT nanofibers in the laminate showed increased flexural strength, with a further increase in flexural strain than the baseline (Fig. 5 (a)). The baseline sample represents a flexural strength of 726.01 \pm 23.83 MPa and with the incorporation of 4 wt% MWCNT ENFs, the flexural strength obtained was

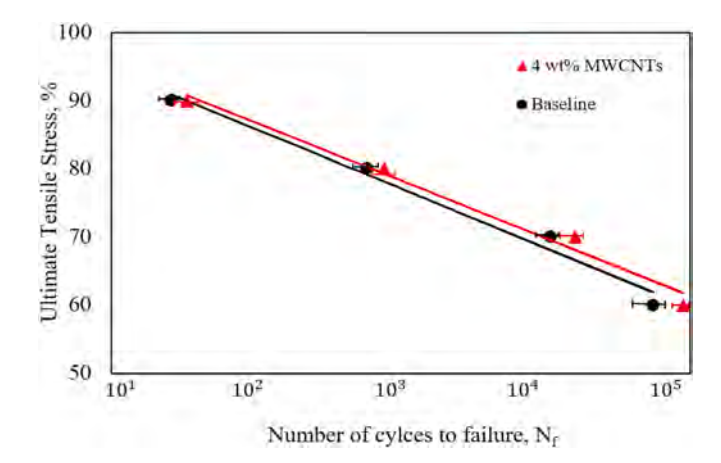


Fig. 4. Short Beam fatigue testing of baseline and enhanced composites with 4 wt% MWCNTs under cyclic loading.

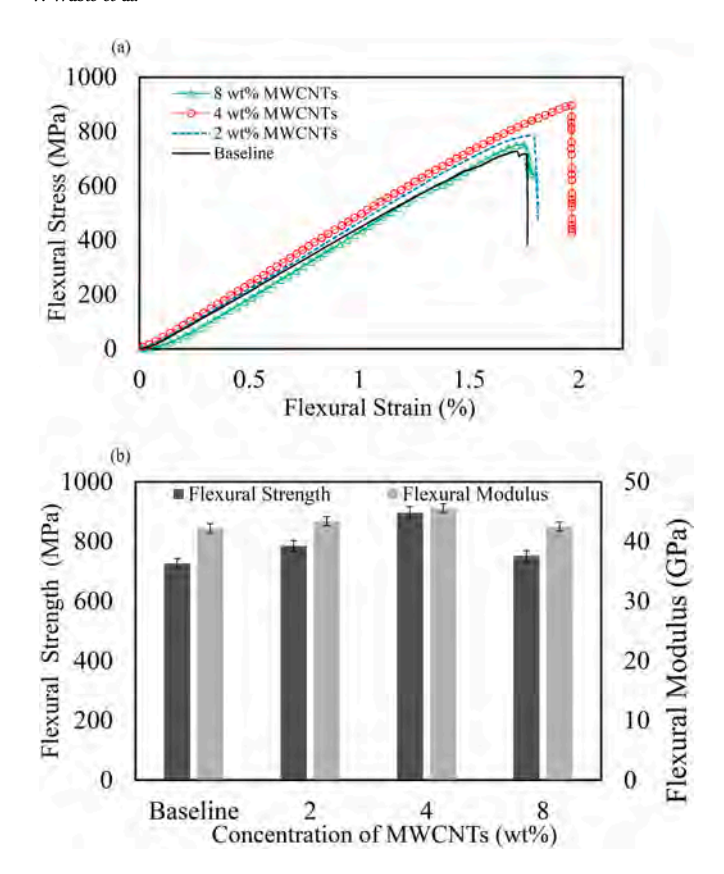


Fig. 5. Baseline vs. 2,4 and 8 wt% MWCNTs composite laminates. (a) Flexural stress-strain curves and (b) Average flexural strength and modulus strength.

 895.98 ± 12.99 MPa. This concentration renders an increase of 23% with respect to the baseline. This demonstrates that nanoreinforcement enables matrix strengthening when adding electrospun MWCNTs between matrices. Furthermore, the electrospun composite laminates indicated increasing 11% of flexural modulus with the 4 wt % MWCNT ENFs as shown in Fig. 5(b). As it has been observed, 4 wt% MWCNTs shows the best performance among the other concentrations, and after the 4 wt% MWCNTs the enhancement rate drops. To elucidate these concentrations, the structural strength of the laminate must be increased, yet the engineering original weight have been not changed predominantly.

Fig. 6 (a) demonstrates that the MWCNTs are uniformly distributed in the nanofibers. To enable a good load transfer from the polymer to the MWCNTs, proper dispersion of MWCNTs is important for improved properties of the composite. The average diameter of MWCNTs was 38 nm, which was much smaller than the electrospun nanofibers (100–500 nm), hence making them good filler materials. In the current study, the MWCNTs were dispersed in a solvent solution. The addition of a small amount of (1:20 of the total solution) Triton-X surfactant has facilitated the better dispersion of MWCNTs [32,55].

The fracture surfaces were observed at high magnification to determine the typical fracture regions, as shown in Fig. 6(b–c). There were significant variations in fracture morphology between the CFRP composites with and without MWCNTs ENFs. This relates to the parameters based on the results of the SBS tests. The matrix in the baseline composites was typically separated from the fibers, as shown by the fiber surfaces (Fig. 6b) revealing poor interfacial adhesion and debonding between the plies. Meanwhile, the matrix material is subjected to a considerable risk of failure and crack propagation. In contrast, the fibermatrix interface in the composite with MWCNT ENFs remain intact even after fracture (Fig. 6c), demonstrating strong interfacial adhesion and the interlaminar failure occurring due to resin cracking and deformation within the CNF rich matrix interlayer. Due to the electrospinning

process, MWCNTs become aligned and consequently provide a better mechanical performance. The detailed study has been discussed earlier in our recent publication [32].

It is widely understood that the ISS of fiber reinforced polymers relies upon each the fiber-matrix interfacial bond and the shear properties of the composite matrix [56]. The electrospun nanofibers present within each layer of the prepreg appear to have functioned as the reinforcement to the matrix, enriched the interface, and improved matrix shear properties. The adhesion of the matrix to the fibers shows a good fiber-matrix interface, which appears to be a result of adding the electrospun MWCNT-epoxy layer. The high-level porosity of the electrospun layer makes the resin to flow easily, maintaining a strong bonding between the two prepreg layers where the nanofibers are added. It is worth noting that electrospun nanofibers hindered the crack initiation and propagation in the 4 wt% MWCNTs composites, resisting higher loading conditions.

3.2. BVID

Minor damage events are hard to identify on the surface of composites. However, formation of such damages on the structures over time can have the same significant structural impact as delamination, matrix cracking and fiber fracture. To minimize these effects, minor damages need to be examined using a BVID test to avoid catastrophic failure. According to the American Society for Testing and Materials definition, BVID damages are classified as those which are visible at fewer than 1.5 m and Visible Impact Damage (VID) are those which visible at 1.5 m [57]. The impact effect at specific energy rates on control and enhanced composites are presented in Fig. 7.

The damaged areas were measured, and results revealed a significant improvement in damage resistance by employing electrospun nanofibers between the prepreg layers of composite. Such that, there is a 7.44 J increase in impact energy absorption by adding 4 wt% MWCNTs/epoxy nanofibers. From this it can be concluded that resistance to delamination is elevated by ~45% in energy absorption on the surface when comparing enhanced composites to control ones. In all cases dented area for the controlled sample was found to be significantly bigger than the 4 wt% MWCNTs reinforced (enhanced) sample. This is due to the presence of nano-reinforcement between the prepreg layers, which appears to be able to dissipate the impact energy. At the energy level of 35.15 J, surface indentation is easily visible, and the enhanced composite enters the VID criteria.

3.3. Thermal conductivity

Heat dissipation is one of the significant properties to be addressed for any material that has the potential to be incorporated in heavy industry applications like aircraft or marine, as poor heat dissipation will reduce the material life and performance. In general, CFRP shows moderate thermal conductivity in the through-the-thickness direction (0.4-0.5 W/m·K) [58] because epoxy resin infused in the CFRP layers exhibits poor thermal conductivity (0.15-0.25 W/m·K) [59,60]. One of the common strategies to enhance the thermal conductivity of CFRP laminates is doping the epoxy resin with nanoparticles that possess high thermal conductivity, including ceramic nanoparticles [61], metal nanopowders [62], and carbon-based fillers [63,64]. Among all these doping materials, carbon nanotubes are found to be the most promising as high conductivity is achieved without compromising laminate thickness and weight. In our work, we have incorporated MWCNT with epoxy resin in low concentration (2,4, and 8 wt%) which help attain high thermal conductivity.

Fig. 8 shows that 2 wt% MWCNT-Epoxy exhibits about 43% increment in thermal conductivity when compared to controlled samples. MWCNT forms a vast conductive network in the resin matrix which ultimately creates a strong connection between carbon fibers of all layers and transfer heat flow easily. It has been also observed 4 and 8 wt

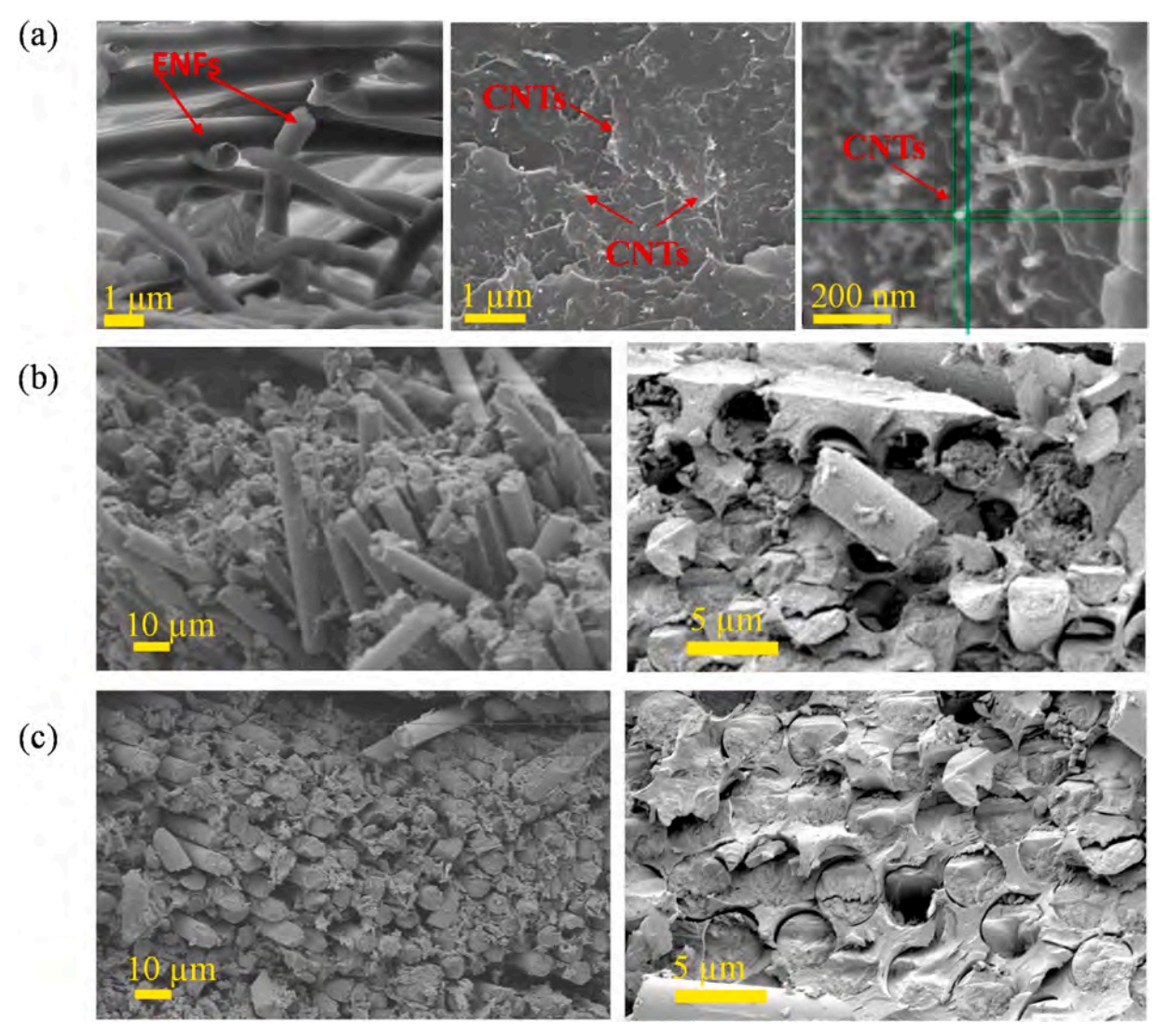


Fig. 6. a) SEM micrographs of the epoxy matrix: Electrospun MWCNTs nanofibers (ENFs) (left), well-dispersed 4 wt% MWCNTs (middle), uniform distribution of randomly oriented MWCNTs inside the structure (right). b) Fracture surface of SBS test specimens without MWCNTs showing fiber/matrix interfacial region at different magnifications. c) Fracture surface of SBS test specimens with 4 wt% MWCNTs at different magnifications demonstrate a more uniform fracture surface.

% MWCNT-epoxy samples experienced roughly 60, and 77% thermal conductivity enhancement, respectively.

3.4. Electrical conductivity and EMI shielding

CFRP composites are prone to lightning damage, unlike conventional aluminum alloys, due to limited electrical conductivity. This is an important property as higher electrical conductivity reduces the damage caused by lightning, especially in aircraft by helping to charge dispersion on the surface. MWCNT is one of the most highly conductive carbonaceous materials. Its addition to the epoxy resin and electrospun nanofibers would be expected to form a conductive path through the entire laminate. Fig. 9(a) shows the results of the electrical resistivity of control and MWCNT-epoxy composites. According to percolation theory, the electrical properties of the composites are assumed to rise exponentially when there is a certain volume of filler material, owing to the tunneling effect of the electrons [65–67]. Similarly, adding MWCNT in epoxy resin is expected to increase electrical conductivity. The electrical conductivity value of the control sample was estimated at 0.0011 \pm 0.0002 S/cm, but adding 2, 4, and 8 wt% MWCNT-epoxy composites increased the thermal conductivity to 0.0058 \pm 0.0009 S/cm, 0.0120 \pm 0.0028 S/cm, and 0.0163 \pm 0.0002 S/cm, respectively.

EMI shielding effectiveness depends on several parameters such as conductivity of the composite matrices, aspect ratio of nanostructured materials, and content of the conductive fillers such as MWCNTs, graphene, etc. [39,68] The high electrical conductivity, large surface area, and large aspect ratio of MWCNTs if properly distributed in the composite materials can help them become a superior candidate for EMI shielding applications [69,70]. The EMI SE mechanism previously reported in literature can be explained as follows. When electromagnetic waves (EMWs) hit the surface of the composites, some of the waves are immediately reflected because of plentiful free electrons [71]. Some of the remaining electromagnetic waves pass through the carbon fibers where they interact with the high density of electron clouds in the matrices and introduce current causing Ohmic losses [72]. The remaining EMWs, after passing through the first layer of MWCNT, encounter the next barrier and the phenomenon of EMW attenuation is repeated. Simultaneously, the inner layer acts as a reflecting surface and gives rise to multiple reflections resulting in further reduction of the total transmission of EMWs.

Increasing in EMI effectiveness can be related to electrical conductivity of specimens [73], and this effect is shown in Fig. 9, where the electrical conductivity of specimens is increased by increase in MWCNTs content, and shielding effectiveness increases continuously with

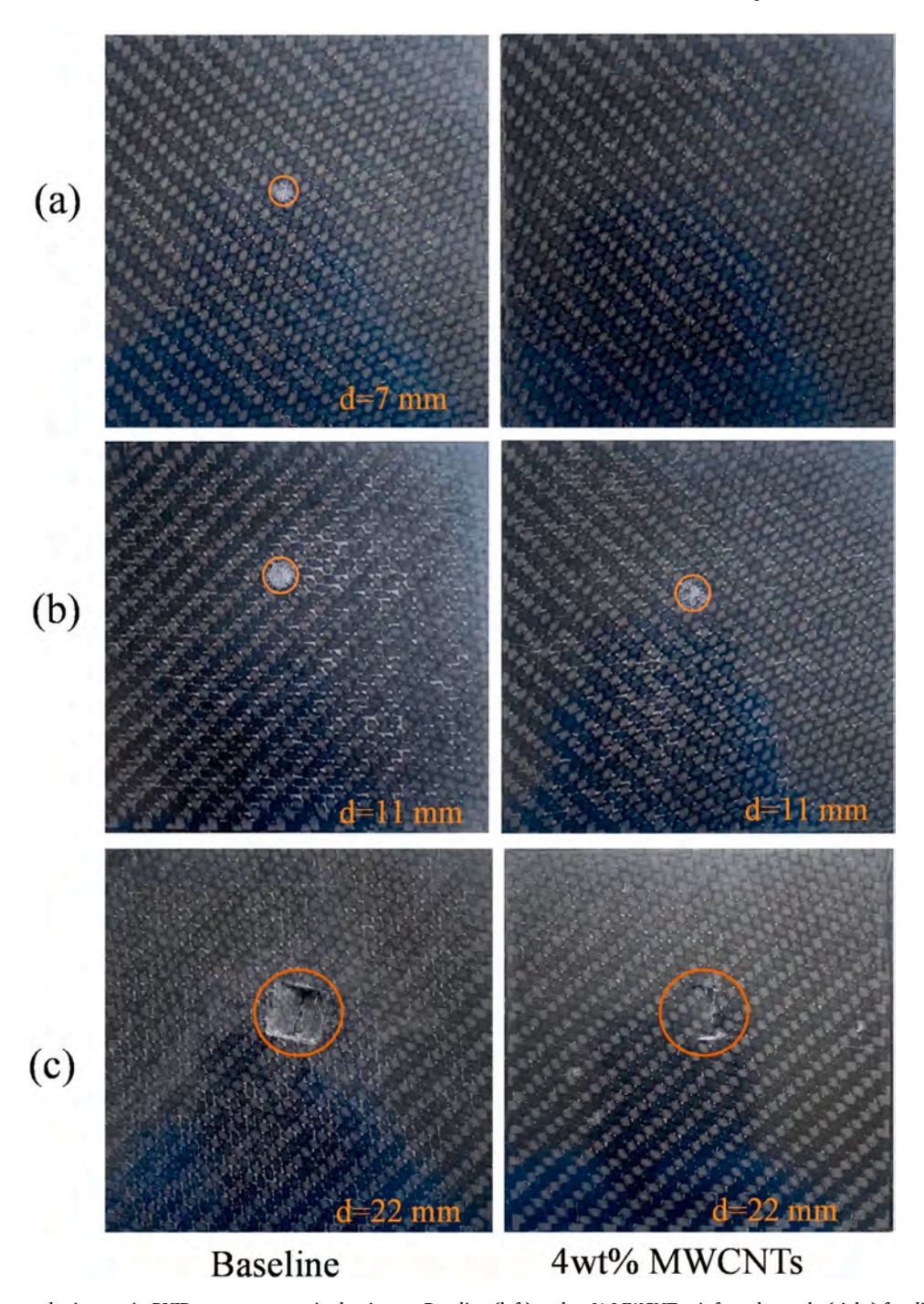


Fig. 7. Dented area due to the impact in BVID test on composite laminates, Baseline (left) and wt% MWCNT reinforced sample (right) for different energy tests a) 16.50 J, b) 23.94 J and c) 35.15 J.

increasing electrical conductivity. Here it was found that the SE value is independent of the frequency in the X-band range and with increasing the MWCNTs content, the EMI SE has gradually increased. From the obtained data it has been shown that the average value for EMI SE reported being 20.46 ± 0.40 dB, 22.5 ± 0.23 dB, 25.18 ± 0.45 dB, and 29.49 ± 0.69 dB for control, 2, 4, and 8 wt%, respectively. Results revealed that inclusion of just 2, 4, and 8 wt% MWCNTs in CFRP composite layers result in approx. 9%, 23%, 44% increase in EMI SE. For many applications, any composite material with a SE_T value close to 30 dB at X-band frequency is regarded as having an appropriate degree of shielding [74].

4. Conclusions

A novel fabrication procedure was successfully presented for nanostructural composites by making the thermoset epoxy resin spinnable. Nanofibers were fabricated by an optimized electrospinning process that resulted in the unidirectional formation of MWCNTs inside the nanofiber's structure. The mechanical properties, including interlaminar shear strength, fatigue, and BVID along with the thermal and electrical conductivity, and EMI shielding of the fabricated composites were evaluated. Results revealed that by incorporating the electrospun nanofiber scaffold, the mechanical properties of the composite were considerably improved. According to the SBS test, ILSS and fatigue performance, at 90% of ultimate static strength, increased by 29% and

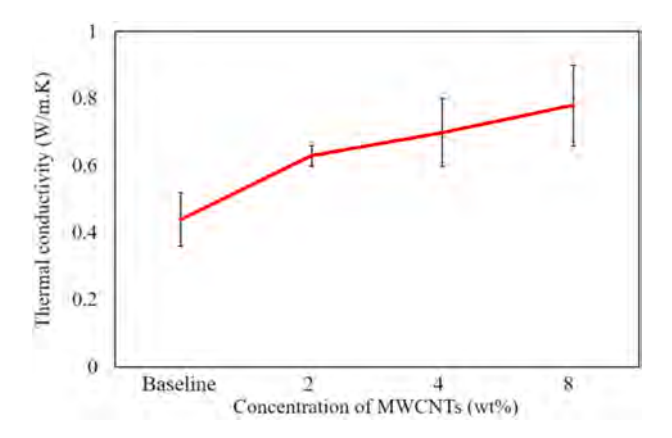


Fig. 8. Thermal conductivity of control and enhanced composite with 2,4,8 wt % MWCNTs.

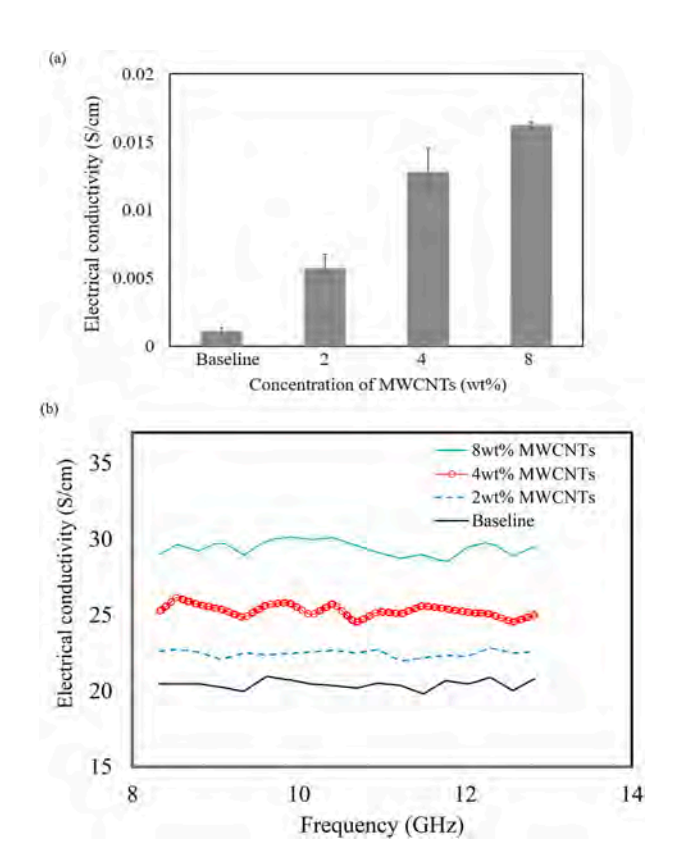


Fig. 9. (a) Through-plane conductivity measured at 100 Hz and (b) EMI Shielding Effectiveness of baseline and different concentration of MWCNTs (wt%).

27%, respectively, by adding 4 wt% MWCNTs/epoxy nanofibers. Furthermore, 23% and 11% improvements were attained for flexural strength and modulus at the enhanced composite with 4 wt% MWCNTs/epoxy. BVID energy was increased significantly by 45% for 4 wt% MWCNTs samples compared to the control composite. Further, the shielding effectiveness of enhanced composite expressively increased by incorporation of highly conductive MWCNTs in CF structure using this method. Comparing all the results from mechanical, thermal, and electrical properties, it was concluded that enhanced composites incorporating 4 wt% MWCNTs/epoxy ENFs have optimum properties, and therefore will be suitable for many high-performance applications.

Author statement

Vidya Wable: Material preparations, mechanical characterization, acquisition of data, drafting the manuscript. Pias K. Biswas: BVID, Electrical and Thermal writing – review, experiment advice and aid. Reza Moheimani: Contributed to mechanical characterization, coordinated revising the manuscript and assistance in response to the reviewers. Nojan Aliahmad: Discussion, SEM characterization, nanocomposite preparation. Peter Omole: Material preparation and lamination. Amanda P. Siegel: Technical advisor and coordination in manuscript preparation. Mangilal Agarwal & Hamid Dalir: Research idea, critical advices for various aspects of the project, supervision.

Declaration of competing interest

The authors declare that this study received funding from Multiscale Integrated Technology Solutions LLC (MITS) as part of NSF awarded STTR grant (#2036490). Amanda P. Siegel, Mangilal Agarwal and Hamid Dalir declare competing interests. Mangilal Agarwal and Hamid Dalir are owners of MITS, and inventors of "manufacturing of submicron carbon nanotube epoxy nanocomposite filaments" (US Patent Pending #62/866,319). Amanda P. Siegel is an owner and Chief Scientific Officer of MITS. The remaining authors declare that the research was conducted in the absence of any commercial or financial relationships that could be construed as a potential conflict of interest.

Acknowledgment

The authors would like to express their gratitude towards the National Science Foundation Small Business Technology Transfer (NSF-STTR) (#2036490) for sponsoring this research; the National Science Foundation Major Research Instrumentation Program (NSF-MRI) (#1229514) for supporting this research for FESEM; National Science Foundation Multidisciplinary Research for Undergraduates in Nanomaterials for Biomedical and Energy Applications (NSF-REU) (#1950672) for supporting Iran Hernandez and her contributions in making nanocomposite nanofilaments; and IUPUI Diversity Scholars Research Program (DSRP) for supporting Peter Omole. This work is also sponsored in part by the Indiana 21st Century Fund and the Indiana Economic Development Corporation. Any opinions, findings, and conclusions or recommendations expressed in this material are those of the author(s) and do not necessarily reflect the views of the National Science Foundation.

References

- Y. Shi, T. Swait, C. Soutis, Modelling damage evolution in composite laminates subjected to low velocity impact, Compos. Struct. 94 (9) (2012) 2902–2913.
- [2] C. Soutis, Fibre reinforced composites in aircraft construction, Prog. Aero. Sci. 41 (2) (2005) 143–151.
- [3] S. Pavlopoulou, S.A. Grammatikos, E.Z. Kordatos, K. Worden, A.S. Paipetis, T. E. Matikas, C. Soutis, Continuous debonding monitoring of a patch repaired helicopter stabilizer: damage assessment and analysis, Compos. Struct. 127 (2015) 231–244
- [4] M.A. Caminero, G.P. Rodríguez, V. Muñoz, Effect of stacking sequence on Charpy impact and flexural damage behavior of composite laminates, Compos. Struct. 136 (2016) 345–357.
- [5] Z. Li, A. Haigh, C. Soutis, A. Gibson, R. Sloan, N. Karimian, Detection and evaluation of damage in aircraft composites using electromagnetically coupled inductors, Compos. Struct. 140 (2016) 252–261.
- [6] Y. Shi, C. Soutis, Modelling transverse matrix cracking and splitting of cross-ply composite laminates under four point bending, Theor. Appl. Fract. Mech. 83 (2016) 73–81.
- [7] S. Rivallant, C. Bouvet, E. Abi Abdallah, B. Broll, J.-J. Barrau, Experimental analysis of CFRP laminates subjected to compression after impact: the role of impact-induced cracks in failure, Compos. Struct. 111 (2014) 147–157.
- [8] B. Ostré, C. Bouvet, C. Minot, J. Aboissière, Experimental analysis of CFRP laminates subjected to compression after edge impact, Compos. Struct. 152 (2016) 767–778.
- [9] M.R. Wisnom, S.R. Hallett, The role of delamination in strength, failure mechanism and hole size effect in open hole tensile tests on quasi-isotropic laminates, Compos. Appl. Sci. Manuf. 40 (4) (2009) 335–342.

- [10] V.J. Hawyes, P.T. Curtis, C. Soutis, Effect of impact damage on the compressive response of composite laminates, Compos. Appl. Sci. Manuf. 32 (9) (2001) 1263–1270.
- [11] X. Zhang, H. Hao, Y. Shi, J. Cui, X. Zhang, Static and dynamic material properties of CFRP/epoxy laminates, Construct. Build. Mater. 114 (2016) 638–649.
- [12] L. Sun, G.L. Warren, J.Y. O'Reilly, W.N. Everett, S.M. Lee, D. Davis, D. Lagoudas, H. J. Sue, Mechanical properties of surface-functionalized SWCNT/epoxy composites, Carbon 46 (2) (2008) 320–328.
- [13] N. Yu, Z.H. Zhang, S.Y. He, Fracture toughness and fatigue life of MWCNT/epoxy composites, Mater. Sci. Eng., A 494 (1) (2008) 380–384.
- [14] J. Wei, T. Vo, F. Inam, Epoxy/graphene nanocomposites processing and properties: a review, RSC Adv. 5 (90) (2015) 73510–73524.
- [15] M. Maghsoudi-Ganjeh, L. Lin, X. Wang, X. Wang, X. Zeng, Computational modeling of the mechanical behavior of 3D hybrid organic-inorganic nanocomposites, J. Occup. Med. 71 (11) (2019) 3951–3961.
- [16] M. Maghsoudi-Ganjeh, L. Lin, X. Wang, X. Zeng, Bioinspired design of hybrid composite materials, Int. J. Soc. Netw. Min. 10 (1) (2019) 90–105.
- [17] R. Cao, J. Wang, S. Zhao, W. Yang, Z. Yuan, Y. Yin, X. Du, N.-W. Li, X. Zhang, X. Li, Self-powered nanofiber-based screen-print triboelectric sensors for respiratory monitoring, Nano Res. 11 (7) (2018) 3771–3779.
- [18] X. Lu, C. Wang, Y. Wei, One-dimensional composite nanomaterials: Synthesis by electrospinning and their applications, Small 5 (21) (2009) 2349–2370.
- [19] B. Wang, Z. Sun, Q. Sun, J. Wang, Z. Du, C. Li, X. Li, The preparation of bifunctional electrospun air filtration membranes by introducing attapulgite for the efficient capturing of ultrafine PMs and hazardous heavy metal ions, Environ. Pollut. 249 (2019) 851–859.
- [20] F. Wu, C. Li, R. Cao, X. Du, High-performance electronic cloth for facilitating the rehabilitation of human joints, ACS Appl. Mater. Interfaces 11 (25) (2019) 22722–22729
- [21] B. Farkas, A. Balogh, R. Cselkó, K. Molnár, A. Farkas, E. Borbás, G. Marosi, Z. K. Nagy, Corona alternating current electrospinning: a combined approach for increasing the productivity of electrospinning, Int. J. Pharm. 561 (2019) 219–227.
- [22] W. Liu, J. Zhang, H. Liu, Conductive bicomponent fibers containing polyaniline produced via side-by-side electrospinning, Polymers 11 (6) (2019) 954.
- [23] P. Vass, E. Hirsch, R. Kóczián, B. Démuth, A. Farkas, C. Fehér, E. Szabó, Á. Németh, S.K. Andersen, T. Vigh, Scaled-up production and tableting of grindable electrospun fibers containing a protein-type drug, Pharmaceutics 11 (7) (2019) 320
- [24] T. Meireman, L. Daelemans, S. Rijckaert, H. Rahier, W. Van Paepegem, K. De Clerck, Delamination resistant composites by interleaving bio-based long-chain polyamide nanofibers through optimal control of fiber diameter and fiber morphology, Compos. Sci. Technol. 193 (2020), 108126.
- [25] N.K. Han, Y.C. Choi, D.U. Park, J.H. Ryu, Y.G. Jeong, Core-shell type composites based on polyimide-derived carbon nanofibers and manganese dioxide for selfstanding and binder-free supercapacitor electrode applications, Compos. Sci. Technol. 196 (2020). 108212.
- [26] M. Wang, D. Li, J. Li, S. Li, Z. Chen, D.-G. Yu, Z. Liu, J.Z. Guo, Electrospun Janus zein–PVP nanofibers provide a two-stage controlled release of poorly water-soluble drugs, Mater. Des. 196 (2020), 109075.
- [27] M. Wang, J. Hou, D.-G. Yu, S. Li, J. Zhu, Z. Chen, Electrospun tri-layer nanodepots for sustained release of acyclovir, J. Alloys Compd. 846 (2020), 156471.
- [28] K. Zhao, S.-X. Kang, Y.-Y. Yang, D.-G. Yu, Electrospun functional nanofiber membrane for antibiotic removal in water, Polymers 13 (2) (2021) 226.
- [29] L. You, Z. Wang, Y. Kang, Y. Zhao, D. Zhang, Experimental investigation of porosity and permeability change caused by salting out in tight sandstone gas reservoirs, J. Nat. Gas Geosci. 3 (6) (2018) 347–352.
- [30] S. Kang, S. Hou, X. Chen, D.-G. Yu, L. Wang, X. Li, G. R Williams, Energy-saving electrospinning with a concentric teflon-core rod spinneret to create medicated nanofibers, Polymers 12 (10) (2020) 2421.
- [31] Z.-M. Huang, Y.-Z. Zhang, M. Kotaki, S. Ramakrishna, A review on polymer nanofibers by electrospinning and their applications in nanocomposites, Compos. Sci. Technol. 63 (15) (2003) 2223–2253.
- [32] N. Aliahmad, P.K. Biswas, V. Wable, I. Hernandez, A. Siegel, H. Dalir, M. Agarwal, Electrospun thermosetting carbon nanotube–epoxy nanofibers, ACS Appl. Polym. Mater. 3 (2) (2021) 610–619.
- [33] A.P. Kishan, E.M. Cosgriff-Hernandez, Recent advancements in electrospinning design for tissue engineering applications: a review, J. Biomed. Mater. Res. 105 (10) (2017) 2892–2905.
- [34] J. Xue, T. Wu, Y. Dai, Y. Xia, Electrospinning and electrospun nanofibers: methods, materials, and applications, Chem. Rev. 119 (8) (2019) 5298–5415.
- [35] Y. Chen, Z. Wang, X. Li, X. Yao, C. Wang, Y. Li, W. Xue, D. Yu, S.Y. Kim, F. Yang, Li metal deposition and stripping in a solid-state battery via Coble creep, Nature 578 (7794) (2020) 251–255.
- [36] X. Li, W. Chen, Q. Qian, H. Huang, Y. Chen, Z. Wang, Q. Chen, J. Yang, J. Li, Y. W. Mai, Electrospinning-based strategies for battery materials, Adv. Energy Mater. 11 (2) (2021), 2000845.
- [37] L.Y. Yeo, J.R. Friend, Electrospinning carbon nanotube polymer composite nanofibers, J. Exp. Nanosci. 1 (2) (2006) 177–209.
- [38] Q. Chen, W. Wu, Y. Zhao, M. Xi, T. Xu, H. Fong, Nano-epoxy resins containing electrospun carbon nanofibers and the resulting hybrid multi-scale composites, Compos. B Eng. 58 (2014) 43–53.
- [39] K. Molnár, G. Szebényi, B. Szolnoki, G. Marosi, L.M. Vas, A. Toldy, Enhanced conductivity composites for aircraft applications: carbon nanotube inclusion both in epoxy matrix and in carbonized electrospun nanofibers, Polym. Adv. Technol. 25 (9) (2014) 981–988.

- [40] U.A. Shakil, S.B.A. Hassan, M.Y. Yahya, S. Nauman, Mechanical properties of electrospun nanofiber reinforced/interleaved epoxy matrix composites—a review, Polym. Compos. 41 (6) (2020) 2288–2315.
- [41] Y. Lin, M. Gigliotti, M.C. Lafarie-Frenot, J. Bai, D. Marchand, D. Mellier, Experimental study to assess the effect of carbon nanotube addition on the through-thickness electrical conductivity of CFRP laminates for aircraft applications, Compos. B Eng. 76 (2015) 31–37.
- [42] Y. Akcin, S. Karakaya, O. Soykasap, Electrical, thermal and mechanical properties of CNT treated prepreg CFRP composites, Mater. Sci. Appl. 7 (9) (2016) 465.
- [43] A. Badakhsh, K.-H. An, B.-J. Kim, Enhanced surface energetics of CNT-grafted carbon fibers for superior electrical and mechanical properties in CFRPs, Polymers 12 (6) (2020) 1432.
- [44] S.L. Ogin, P. Potluri, 1 textile-reinforced composite materials, in: A.R. Horrocks, S.C. Anand (Eds.), Handbook of Technical Textiles (second ed.), Woodhead Publishing2016, pp. 1-26.
- [45] R. Moheimani, R. Sarayloo, H. Dalir, Failure study of fiber/epoxy composite laminate interface using cohesive multiscale model, Adv. Compos. Lett. 29 (2020), 2633366X20910157.
- [46] S. Naeem, V. Baheti, V. Tunakova, J. Militky, D. Karthik, B. Tomkova, Development of porous and electrically conductive activated carbon web for effective EMI shielding applications, Carbon 111 (2017) 439–447.
- [47] V. Šafářová, M. Tunák, M. Truhlár, J. Militký, A new method and apparatus for evaluating the electromagnetic shielding effectiveness of textiles, Textil. Res. J. 86 (1) (2015) 44–56.
- [48] Y. Tan, H. Luo, X. Zhou, S. Peng, H. Zhang, Dependences of microstructure on electromagnetic interference shielding properties of nano-layered Ti3AlC2 ceramics, Sci. Rep. 8 (1) (2018) 7935.
- [49] X. Ni, C. Furtado, E. Kalfon-Cohen, Y. Zhou, G.A. Valdes, T.J. Hank, P.P. Camanho, B.L. Wardle, Static and fatigue interlaminar shear reinforcement in aligned carbon nanotube-reinforced hierarchical advanced composites, Compos. Appl. Sci. Manuf. 120 (2019) 106–115.
- [50] P.-C. Ma, S.-Y. Mo, B.-Z. Tang, J.-K. Kim, Dispersion, Interfacial interaction and reagglomeration of functionalized carbon nanotubes in epoxy composites, Carbon 48 (6) (2010) 1824–1834.
- [51] S. Zainuddin, A. Fahim, T. Arifin, M.V. Hosur, M.M. Rahman, J.D. Tyson, S. Jeelani, Optimization of mechanical and thermo-mechanical properties of epoxy and E-glass/epoxy composites using NH2-MWCNTs, acetone solvent and combined dispersion methods, Compos. Struct. 110 (2014) 39–50.
- [52] Y. Iwahori, S. Ishiwata, T. Sumizawa, T. Ishikawa, Mechanical properties improvements in two-phase and three-phase composites using carbon nano-fiber dispersed resin, Compos. Appl. Sci. Manuf. 36 (10) (2005) 1430–1439.
- [53] M. Sánchez, M. Campo, A. Jiménez-Suárez, A. Ureña, Effect of the carbon nanotube functionalization on flexural properties of multiscale carbon fiber/epoxy composites manufactured by VARIM, Compos. B Eng. 45 (1) (2013) 1613–1619.
- [54] Y. Rostamiyan, A. Fereidoon, M. Rezaeiashtiyani, A. Hamed Mashhadzadeh, A. Salmankhani, Experimental and optimizing flexural strength of epoxy-based nanocomposite: effect of using nano silica and nano clay by using response surface design methodology, Mater. Des. 69 (2015) 96–104.
- [55] M. Li, Y. Gu, Y. Liu, Y. Li, Z. Zhang, Interfacial improvement of carbon fiber/epoxy composites using a simple process for depositing commercially functionalized carbon nanotubes on the fibers, Carbon 52 (2013) 109–121.
- [56] J.-K. Kim, Y.-W. Mai, Y.-W. Mai, Chapter 8 improvement of interlaminar fracture toughness with interface control, in: J.-K. Kim, Y.-W. Mai, Y.-W. Mai (Eds.), Engineered Interfaces in Fiber Reinforced Composites, Elsevier Science Ltd, Oxford, 1998, pp. 329–365.
- [57] H. Park, C. Kong, Experimental study on barely visible impact damage and visible impact damage for repair of small aircraft composite structure, Aero. Sci. Technol. 29 (1) (2013) 363–372.
- [58] S.L. Chung, J.S. Lin, Thermal conductivity of epoxy resin composites filled with combustion synthesized h-BN particles, Molecules 21 (5) (2016).
- [59] H.S. Kaufman, Handbook of epoxy resins. Henry lee and Kris Neville, J. Appl. Polym. Sci. 14 (1) (1970) 253, 253.
- [60] R.D. Sweeting, X.L. Liu, Measurement of thermal conductivity for fibre-reinforced composites, Compos. Appl. Sci. Manuf. 35 (7) (2004) 933–938.
- [61] K.W. Garrett, H.M. Rosenberg, The thermal conductivity of epoxy-resin/powder composite materials, J. Phys. Appl. Phys. 7 (9) (1974) 1247–1258.
- [62] C. Chen, Y. Tang, Y.S. Ye, Z. Xue, Y. Xue, X. Xie, Y.-W. Mai, High-performance epoxy/silica coated silver nanowire composites as underfill material for electronic packaging, Compos. Sci. Technol. 105 (2014) 80–85.
- [63] F.H. Gojny, M.H.G. Wichmann, B. Fiedler, I.A. Kinloch, W. Bauhofer, A.H. Windle, K. Schulte, Evaluation and identification of electrical and thermal conduction mechanisms in carbon nanotube/epoxy composites, Polymer 47 (6) (2006) 2036–2045.
- [64] W. Zhou, Effect of coupling agents on the thermal conductivity of aluminum particle/epoxy resin composites, J. Mater. Sci. 46 (11) (2011) 3883–3889.
- [65] S.Y. Kim, Y.J. Noh, J. Yu, Prediction and experimental validation of electrical percolation by applying a modified micromechanics model considering multiple heterogeneous inclusions, Compos. Sci. Technol. 106 (2015) 156–162.
- [66] Y.J. Noh, S.Y. Pak, S.H. Hwang, J.Y. Hwang, S.Y. Kim, J.R. Youn, Enhanced dispersion for electrical percolation behavior of multi-walled carbon nanotubes in polymer nanocomposites using simple powder mixing and in situ polymerization with surface treatment of the fillers, Compos. Sci. Technol. 89 (2013) 29–37.
- [67] Y.J. Noh, H.-I. Joh, J. Yu, S.H. Hwang, S. Lee, C.H. Lee, S.Y. Kim, J.R. Youn, Ultrahigh dispersion of graphene in polymer composite via solvent freefabrication and functionalization, Sci. Rep. 5 (1) (2015) 9141.

- [68] Z. Liu, G. Bai, Y. Huang, Y. Ma, F. Du, F. Li, T. Guo, Y. Chen, Reflection and absorption contributions to the electromagnetic interference shielding of singlewalled carbon nanotube/polyurethane composites, Carbon 45 (4) (2007) 821–827.
- [69] C.-S. Zhang, Q.-Q. Ni, S.-Y. Fu, K. Kurashiki, Electromagnetic interference shielding effect of nanocomposites with carbon nanotube and shape memory polymer, Compos. Sci. Technol. 67 (14) (2007) 2973–2980.
- [70] M.H. Al-Saleh, U. Sundararaj, Electromagnetic interference shielding mechanisms of CNT/polymer composites, Carbon 47 (7) (2009) 1738–1746.
- [71] T.-W. Lee, S.-E. Lee, Y.G. Jeong, Carbon nanotube/cellulose papers with high performance in electric heating and electromagnetic interference shielding, Compos. Sci. Technol. 131 (2016) 77–87.
- [72] H.-B. Zhang, Q. Yan, W.-G. Zheng, Z. He, Z.-Z. Yu, Tough Graphene—Polymer microcellular foams for electromagnetic interference shielding, ACS Appl. Mater. Interfaces 3 (3) (2011) 918–924.
- [73] J. Wang, Y. Kazemi, S. Wang, M. Hamidinejad, M.B. Mahmud, P. Pötschke, C. B. Park, Enhancing the electrical conductivity of PP/CNT nanocomposites through crystal-induced volume exclusion effect with a slow cooling rate, Compos. B Eng. 183 (2020), 107663.
- [74] M.G. Jang, S.C. Ryu, K.J. Juhn, S.K. Kim, W.N. Kim, Effects of carbon fiber modification with multiwall CNT on the electrical conductivity and EMI shielding effectiveness of polycarbonate/carbon fiber/CNT composites, J. Appl. Polym. Sci. 136 (14) (2019), 47302.